LAWRENCE
LIVERMORE
NATIONAL
LABORATORY

LLNL-JRNL-764337

Evolution of Microstructure and Mechanical Properties of Selective Laser Melted Ti-5Al-5V-5Mo-3Cr After Isothermal Heat Treatments

H. D. Carlton, K. D. Klein, J. W. Elmer

December 18, 2018

Science and Technology of Welding and Joining

Disclaimer

Evolution of Microstructure and Mechanical Properties of Selective Laser Melted Ti-5Al-5V-5Mo-3Cr After Isothermal Heat Treatments

Holly D. Carlton[1], Kyle D. Klein[1], John W. Elmer[1]

[1]Materials Engineering Division, Lawrence Livermore National Laboratory, 7000 East Avenue, L-342, Livermore, CA 94550, USA

Corresponding author email: Carlton4@llnl.gov

Abstract

Titanium alloy Ti5553 (Ti-5Al-5Mo-5V-3Cr) is an excellent candidate for structural applications and additive manufacturing processes, since, unlike Ti6Al4V, when built via selective laser melting and/or post additive manufactured welding, it maintains a near-beta microstructure that is both ductile and high strength. Another feature is that Ti5553 properties are adaptable through post build heat treatment. This study explores the heat treatability of selective laser melted Ti5553 at low temperatures and temperatures approaching the β–transus. Results show strength increases while maintaining ductility at high temperatures (700-800°C), but embrittlement occurs at intermediate temperatures (400-600°C) likely due to changes in volume fraction and morphology of the α-phase. Here, microstructure and x-ray diffraction data are reported after heat-treating to better understand this mechanical response.

IM Release #: LLNL-JRNL-764337

Keywords:
X-ray Diffraction, Mechanical Properties, Beta-Titanium Alloys, Additive Manufacturing, Welding, Selective Laser Melting, Metals, Heat Treatment

Introduction

Ti5553 (Ti-5Al-5Mo-5V-3Cr, weight fraction%) is a heat treatable metastable-beta titanium-alloy that shows promise in the aerospace, automotive, and biomedical industries for structural applications due to the high strength and low density. This relatively new β-stabilized alloy provides an alternative to the more commonly used α/β alloy Ti-6Al-4V (Ti64), and can provide strength, ductility, fatigue resistance, and toughness advantages over other β-stabilized alloys [1-3]. New applications for Ti5553 may include additive manufacturing (AM) and/or joining of components, especially since Ti5553 is being considered for large components for aircraft structures. Because of this, the weldability of Ti5553 has been studied by electron beam [1, 2], laser beam [4] and other welding methods [5]. These studies show that Ti5553 welds have characteristics similar to the base metal with respect to hardness, microstructure, and cross-weld tensile properties. However, welding and AM processing can result in modifications to the microstructure and properties due to the metastable nature of Ti5553. For example, precipitation of α–phase can occur in the portions of the heat affected zone (HAZ) that have reached temperatures close to the β-transus, or dissolution of preexisting base metal α-phase precipitates can occur in the HAZ regions that exceed the β-transus temperature [1]. The extent of these phase transformations in Ti5553 also depends on the cooling rate and thermal history of the part being built [6], which depends on the specific AM or weld processing conditions.

Selective laser melting (SLM) is one AM process that directly builds 3D components from alloy powder feed sources [7]. SLM produces parts layer by layer from a powder bed, and in essence consists of many small overlapping welds, enabling structures to be built in unique geometries more efficiently than by conventional processing methods and often producing weld-like microstructures. To date, there has been a substantial amount of AM work on titanium alloys such as Ti64 [7-9], but it is only recently that Ti5553 is being explored as an SLM alloy [10-12]. Unlike Ti64, Ti5553 when processed by SLM is metastable β-phase due to the large additions of BCC stabilizers, V, Mo, and Cr, that allow for the microstructure to retain β upon fast cooling inherent to the SLM process. This creates a microstructure with the possibility for post build heat treating to enhance, or modify, the properties of AM Ti5553 parts differently than other titanium alloys by producing a range of microstructures with different ratios and morphologies of both the α and β-phase. However, since the mechanical properties are very sensitive to minor processing changes, it is very important to investigate AM Ti5553 for microstructural changes with heat treatment.

The strength and ductility of additively manufactured Ti64 is well known, and is typically reported to be around 1100 MPa and 6%, respectively [7, 8]. However, there is a large variation in properties depending on the processing parameters and sample orientation [9], and cracking of thick additively manufactured Ti64 components is a concern [7]. Ti5553 on the other hand possesses higher ductility, but with lower as-built hardness and strength than Ti64 [11]. These attributes help to minimize distortion, residual stress, and cracking that can accompany thick AM Ti64 part builds. In addition, Ti5553 has the ability to strengthen via both solid-solution

mechanisms in the single phase, and precipitation strengthening of α–phase (HCP) at temperatures below the β-transus (BCC) of approximately 840°C [13-15]. This creates an opportunity for post AM heat treating of Ti5553 to strengthen it to Ti64 values or possibly higher [15], thus making it an attractive alternative to Ti64 as an AM alloy.

Experimental Procedures

In this study, SLM of Ti5553 was investigated as a function of post AM heat treating conditions ranging in temperature between 300°C and 800°C (with a hold time of 1 hour), where little experimental data exists for SLM Ti5553. Samples were built using a Concept Laser M2 powder bed fusion machine. Prior to entering the SLM machine, the powder was fully characterized for composition, which was determined by x-ray fluorescence (XRF) and inert gas fusion (IGF), and particle size, which was determined by the Malvern Morphologi G3 under 20x magnification. The composition is reported in Table 2 and is in line with what is expected with Ti5553. The mean Circular Equivalence (CE) diameter for the Ti5553 powder is 24.29 ± 9.58μm. CE is a standard reporting value for diameter, which equates the projected area of a particle to the area of a circle.

AM Ti5553 plates, used as the starting material for mechanical, X-ray diffraction (XRD) and metallography samples, were built using a checkerboard pattern, meander and contour on, layer thickness of 30 μm, laser power of 100 W, and laser speed of 600 mm/s with the sharpest focal spot diameter (~50 um). The SLM chamber was purged with argon gas that contained 0.2-0.3% oxygen during the build. A plate of AM Ti5553 was machined into 6 rectangular blocks, with dimensions 15 mm x 60 mm (the build direction) x 6 mm, and built at a 30° angle relative to the x-axis of the build plate. Five of the blocks were then used for isothermal heat treatments from 400-800°C (temperatures are presented in Table 1) under vacuum for one hour followed by a furnace cool to room temperature. It is important to note that all the samples were initially stress relieved prior to removal from the build plate. The stress relief was performed at 300°C for 1 hour and unlike the additional 400°C-800°C isothermal heat treatments, was inert gas cooled with flowing argon. Metallography and XRD samples were then cut from each block and electrical discharge machining (EDM) was used to prepare immersion density and tensile samples.

Metallography was performed to determine microstructural changes after isothermal heat treatment. These samples were prepared in the same orientation as the tensile bar gauge width (perpendicular to the build direction) and subjected to grinding/polishing with the final step being an attack polish using a 1:1 volumetric mixture of 10% NaOH solution and colloidal silica suspension. Scanning electron microscopy (SEM) was then performed on the polished samples using a Phenom ProX microscope. Vickers microhardness measurements (6 per heat treatment group) were also performed on the polished samples using a 50g load.

XRD was used to determine the phases present within each sample group after heat treatment using a Bruker D8 Discover diffractometer with a Cu Kα (1.54 Å) source operated at 40kV and 40mA current. Samples used in XRD measurements were oriented 90° from the tensile gage section along the build direction and 6mm direction of the blocks.

The tensile samples were scaled down from ASTM E8, maintaining a 4:1 ratio of length-to-width, with a gauge length of 10 mm, width of 2.5 mm, and thickness of 1 mm. In addition, tensile samples were machined with the long axis along the 60 mm dimension of the blocks and the gauge length along the build direction, as indicated in Figure 3b. Three to four samples from each heat treatment group were tested quasi-statically in tension on an Instron 8562 electromechanical load frame at room temperature with a strain rate of 10^{-3}/s and displacement was measured using two extensometers. Only one sample was tested using a laser extensometer from group 3 to compare to extensometer results. This sample is still included in the tensile results figure (Fig. 3) and shows wavy stress versus strain behavior. Modulus was not counted for this sample, but strain to failure and ultimate strength are still included in the table statistics (Table 1). A similar setup is described in more detail here [16]. SEM images of the fracture surfaces of tensile bars from each heat treatment group were taken using a tungsten tip FEI Quanta 200 microscope.

Results and Discussion

In the present study, microstructural changes that occur after isothermal heat treatments up to the beta-transus are investigated in SLM Ti5553 and compared to mechanical properties and fractography results. For all Ti5553 heat treatment groups the SEM metallographs reveal a primarily equiaxed β-grain microstructure. Throughout the groups there are minimal regions of unfused powder particles and porosity is negligible. The porosity is similar to what has been observed in high density AM metal [17]. This perceived high density is supported by immersion density measurements of >99% for each heat treatment group. Immersion density measurements were calculated using Archimedes principle. All 6 groups had densities within the range of 4.61-4.62 g/cc; here full density is considered 4.65 g/cc [18]. It should be noted that this study reports on overall bulk density and does not show the porosity distribution related to the overall density. As shown in the literature, porosity distribution and morphology plays a large role in mechanical properties [17] and could lead to anisotropic properties, especially concerning for SLM metals where small porosity is commonly seen. Based on the SEM micrographs (Figure 1), at 600°C the α-phase is observed to precipitate both within β grains and along the β grain boundaries. As the heat treatment temperature increases from 600°C to 700°C and 800°C, there is an increase in the size of α particles from the nanometer scale at 600°C to the micron scale at 800°C. At 800°C, the microstructure consists of 25% α phase using an area approximation (Figure 1c). In addition, it should be noted that while α was not detected with SEM at temperatures below 600°C, the phase may still be present in the microstructure for lower temperature heat treatments, but below the resolution limit of the microscope. The presence of α phase in samples treated below 600°C was investigated further using XRD.

The evolution of the diffraction spectrum after different heat treatments is presented in Figure 2. As shown in the figure, high intensity diffraction peaks corresponding to the β phase are present in the Ti5553 sample at room temperature and also when subject to all of the isothermal heat

treatments. However, this tells a more complete story than just the SEM micrographs alone (Figure 1), where α is shown to appear first at 600°C. According to the XRD spectra (Figure 2), α and β are both clearly present in the microstructure for the 500°, 600°, 700° and 800° heat treatment samples. At 400°C it has been previously reported that both α and ω can be present within the microstructure [21]. While evidence for the presence of ω cannot be seen in the 400°C sample here, there are peaks shown in Figure 2c and Figure 2e near α locations, but the reason for their angular shifts relative to the 500-800°C spectra is unknown. Lastly, the 300°C sample corresponds to a heat treatment temperature at which ω has been reported stable for long heat treatment times [20]. While high intensity β peaks are present in this sample, it is possible that several peaks such as the asymmetric peak in Figure 2b near (200) β and the low intensity peak in Figure 2d may correspond to the presence of ω. Further investigation is needed to fully verify the microstructure for the samples heat treated at lower temperatures.

As mentioned previously, one interesting feature of the XRD spectra is the asymmetry of the peak near (200) β, which may be due to several different microstructural characteristics, such as local compositional differences in the β phase or the presence of non-equilibrium phases, like ω-phase. A similar asymmetry has been observed by Jones et al. for as-quenched Ti5553 [19]. The ω-phase was first reported as existing in Ti-V alloys in Frost et al. [20], which reported on the influence of the ω-phase on precipitation of the α-phase, however a recent study by Zheng at al. [21] observed that the ω-phase played essentially no direct role in precipitating or nucleating α. Isothermal aging treatment at 300°C has been reported to promote ω-phase [22]. Specifically, the β-phase decomposes via a shuffle transformation and the {111} planes of the BCC crystal collapse along the <111> direction, resulting in athermal ω and the transformation is thought to be completed upon aging at low temperature into isothermal ω [15, 23]. The ω-phase, which is very sensitive to cooling and heating rates [24] , usually occurs as particles that are 5-10 nm in diameter and has been reported to have hexagonal symmetry. ω-phase is suspected to strongly influence properties and be associated with embrittlement [15, 23, 25, 26], however it is difficult to detect with XRD spectra since many of the characteristic diffraction peaks for the ω phase often overlap with β peak locations, as shown in Figure 2a, and are too small to detect with SEM. Further investigation into the time and temperature-dependent stability of the different phases along with high resolution imaging to detect intermediate phases at temperatures below 500°C are recommended to fully understand the effects on mechanical behavior.

In addition, the two-theta location of the β peaks (Fig. 2b) in the diffraction spectra is shown to shift as a function of heat treatment temperature. It has been reported in literature that as the β phase becomes enriched with β-stabilizing elements, there is an associated decrease in the β lattice parameter [27]. Since enrichment of the β phase has been shown to occur during α precipitation [22, 27, 28], shifting of the β to higher angles in the XRD spectra may suggest increasing volume fractions of α within the microstructure. Another factor that could be contributing the peak shift is residual stresses in the SLM Ti5553 microstructure that are not fully recovered from the heat treatment. A similar shift was shown to occur with Ti64, where the lattice parameter of β was shown to decrease at stress relieving temperatures around 450°C, but increased at higher temperatures as a result of phase transformation [29, 30]. Other factors that could affect the shift

of the Ti5553 peaks could be the presence of non-equilibrium phases that overlap with the β peaks and strain in the β lattice near non-equilibrium phases, like the presence of ω-phase [15, 28].

Another phase that greatly affects the mechanical properties, is the α–phase, via a precipitation hardening mechanism. Specifically, for β-titanium alloys the high strength is often controlled not by the β phase but by largely by the distribution and morphology of the α phase. Ivanasishin et al. [31] found that fine plate-like α lathes contribute to high strength, since that α phase morphology induces a large number of α/β interfaces which hinder dislocation motion. Since the α– phase is also more brittle than the β-phase due to limited slip systems for the HCP crystal system, the XRD spectra and metallography suggests a variation in strength/ductility should be expected between sample groups due to differing volume % and morphology of α phase in the microstructure. Therefore, in order to investigate the effects of microstructural changes on the mechanical behavior, uniaxial tensile mechanical tests were performed on all the heat treatment groups.

The engineering stress-strain response of the different isothermal heat treatment groups tested at room temperature are shown in Figure 3a, and a photograph of a representative tensile sample is shown in Figure 3b. The values for Young's modulus, yield strength, ultimate tensile strength, and strain to failure are report in Table 1. It should be noted that the strain to failure specified includes the elastic and plastic region. As expected for Ti alloys there is very little work hardening behavior. For SLM Ti5553 heat-treated at 300°C the average ultimate strength is 824 MPa and the strain to failure is 17%. Samples heat-treated between 400-500°C possess the largest ultimate strengths (maximum strength of nearly 1400 MPa), but exhibited the most brittle behavior (strain to failure fell to <2%). Samples heat-treated at higher temperatures (600-800°C) exhibited decreasing ultimate strengths relative to the 400 and 500°C heat treatment groups and increasing strain to failures with increasing temperatures. Figure 4 displays the trend in strength and strain to failure as a function of heat treatment temperature. The 700°C appears to have the optimal combination of yield strength and strain to failure, with 1000 MPa and 14% strain to failure, however the standard deviation in strain to failure is high for both the 700 and 800°C groups. There are several reasons that could explain the scatter in ductility for the high temperature heat treatment groups (700, 800°C), specifically, machining-induced sample abnormalities such as out-of-plane curvature that resulted from machining the thin samples, as well as differences in porosity from the SLM build may be contributing factors.

Following tensile tests, fractography was performed on samples from each heat treatment group in order to further evaluate the critical changes in deformation behavior observed in the stress-strain curves from Figure 3. The fractography is presented in Figure 5 and shows a change in primary failure mode from ductile at 300°C, to brittle (400-600°C), and back to ductile (700- 800°C) as heat treatment temperature increases. Specifically, dimpling indicative of void coalescence and significant plastic deformation is observed at 300°C. Samples heat-treated at 400-600°C shows a mixed mode fracture, with primarily brittle features and limited dimpling present. Finally, widespread dimpling indicative of ductile failure once again becomes visible for the 700-800°C samples with some secondary cracks seen throughout the fracture surface on several of the heat

treatment samples as indicated in Figure 3. Specifically, it should also be noted that unfused powder particles, pores, and cracks were also present on the fracture surfaces of some samples. Such defects could explain some of the variance in the measured mechanical properties that were observed within each sample group.

As previously mentioned, SLM Ti5553 is a great candidate for large structural parts, however the part size is often limited to the build volume of the SLM powder bed machine. This presents a need to be able to weld AM Ti5553 parts together to create structurally sound components. Future studies on Ti5553 AM parts will include laser welding SLM Ti5553 in different joint configurations and investigating the microstructure and mechanical properties of the welded material. This is especially important because previous work [1] on electron beam welded Ti5553 shows good ductility at 11% elongation, in contrast to other work that showed embrittlement in the as welded condition [32]. Initial studies performed at LLNL [25] show that pulsed laser welds in 3 mm thick SLM Ti5553 AM plates have uniform hardness with no significant difference between the fusion zone, heat affected zone and AM base metal as summarized in Table 3. Thus one would expect the weld fusion zone to have similar tensile properties as to the base metal that was stress relieved at 300°C. An optical micrograph showing a cross sectional view of the welded coupon is shown in Fig. 6a. The microstructure of the weld fusion zone is similar to the base metal, but with slightly different β grain size and morphology, having columnar grains in the fusion zone. Porosity is evident in the base material, and also was carried into the weld zone. Porosity such as this is often present in SLM parts, and may explain the variations in strain to failure observed in the tensile curves shown in Fig. 3. The feasibility of welding larger SLM parts together with a complicated step-joint geometry was demonstrated. Figure 6b shows one of the practice parts that joins two Ti5553 SLM components with an internal lattice structure. Future tensile tests are planned to compare the mechanical properties of pulsed laser welded SLM Ti5553 [33].

Conclusions

In summary, SLM Ti5553 is a great candidate for novel structural applications due to the heat treatability that enables tailoring of the microstructure to produce specific desirable properties. It has been demonstrated that a wide range of strengths and elongations can be obtained by subjecting as built SLM Ti-5553 to a short isothermal heat treatment. It is recommended that with respect to the heat treatment process, caution be used for heat-treating between 300-600°C, which is a common stress-relief temperature range for titanium alloys. Severe embrittlement was observed for heat treating temperatures between 400-500°C where the ductility decreased from ~17% (at 300°C) to less than 2%. It is not clear the reason for such high strength and low ductility at these temperatures, but this may be due to the presence of fine α precipitates, since it appears that the ω-phase fully transforms to α around the same time that embrittlement occurs. Higher heat treating temperatures are associated with increases in ductility, but with a decrease in yield and ultimate tensile strengths. Although there is still significant α in the microstructure at these higher temperatures, the morphology and volume fractures appear to change resulting in a high strength and high ductility α/β microstructure. In conclusion, further investigation into the

compositional variance of the β phase throughout the heat treatment process, defect density of the as-built material, and the time-temperature stability of additional phases such as ω is needed to fully explain the observed mechanical behavior and microstructural evolution of the alloy.

References

1. Sabol, J.C., et al., *Localized tensile strain distribution and metallurgy of electron beam welded Ti–5Al–5V–5Mo–3Cr titanium alloys.* Journal of Materials Processing Technology, 2012.
2. Pasang, T., et al., *Metallurgy and deformation of electron beam welded similar titanium alloys.* AIP Conference Proceedings, 2012.
3. Shekhar, S., et al., *Effect of solution treatment and aging on microstructure and tensile properties of high strength β titanium alloy, Ti–5Al–5V–5Mo–3Cr.* Materials & Design, 2015.
4. Sánchez-Amaya, J., et al., *Microstructure and Mechanical Properties of Ti5553 Butt Welds Performed by LBW under Conduction Regime*. Vol. 7. 2017. 269.
5. Pasang, T., et al., *Comparison of Ti-5Al-5V-5Mo-3Cr Welds Performed by Laser Beam, Electron Beam and Gas Tungsten Arc Welding.* Procedia Engineering, 2013.
6. Kar, S.K., et al., *Quantitative microstructural characterization of a near beta Ti alloy, Ti-5553 under different processing conditions.* Materials Characterization, 2013.
7. DebRoy, T., et al., *Additive manufacturing of metallic components – Process, structure and properties.* Progress in Materials Science, 2018.
8. Zhao, X., et al., *Comparison of the microstructures and mechanical properties of Ti–6Al–4V fabricated by selective laser melting and electron beam melting*. Vol. 95. 2015.
9. Keist, J. and T. Palmer, *Role of geometry on properties of additively manufactured Ti-6Al-4V structures fabricated using laser based directed energy deposition*. Vol. 106. 2016.
10. Schwab, H., et al., *Processing of Ti-5553 with improved mechanical properties via an in-situ heat treatment combining selective laser melting and substrate plate heating.* Materials & Design, 2017.
11. Schwab, H., et al., *Microstructure and mechanical properties of the near-beta titanium alloy Ti-5553 processed by selective laser melting.* Materials & Design, 2016.
12. Zopp, C., et al., *Processing of a metastable titanium alloy (Ti-5553) by selective laser melting.* Ain Shams Engineering Journal, 2017.
13. Xu, S.-h., et al., *Microstructural evolution and mechanical properties of Ti–5Al–5Mo–5V–3Cr alloy by heat treatment with continuous temperature gradient.* Transactions of Nonferrous Metals Society of China, 2018.
14. Dehghan-Manshadi, A. and R.J. Dippenaar, *Development of α-phase morphologies during low temperature isothermal heat treatment of a Ti–5Al–5Mo–5V–3Cr alloy.* Materials Science and Engineering: A, 2011.
15. Sabol, J., et al., *Confirmation of the ω-phase in electron beam welded Ti–5Al–5V–5Mo–3Cr by high-resolution scanning transmission electron microscopy: An initial investigation into its effects on embrittlement.* Scripta Materialia, 2014.
16. Elmer, J.W., et al., *Microstructure and Mechanical Properties of 21-6-9 Stainless Steel Electron Beam Welds.* Metallurgical and Materials Transactions A, 2017.
17. Carlton, H.D., et al., *Damage evolution and failure mechanisms in additively manufactured stainless steel.* Materials Science and Engineering: A, 2016.
18. Fanning, J.C., *Properties of TIMETAL 555 (Ti-5Al-5Mo-5V-3Cr-0.6Fe).* J. of Materi Eng and Perform, 2005.

19. Jones, N., et al., *Thermomechanical processing of Ti–5Al–5Mo–5V–3Cr*. Vol. 490. 2008. 369-377.
20. Frost, P.D., et al., Trans. AMS, 1954.
21. Zheng, Y., et al., *The role of the ω phase on the non-classical precipitation of the α phase in metastable β-titanium alloys*. Vol. 111. 2015.
22. Coakley, J., et al., *Precipitation Processes in the Beta-Titanium Alloy Ti-5Al-5Mo-5V-3Cr*. Vol. 646. 2015. 946.
23. G. Lutjering and J.C. Williams, *"Titanium" Engineering Materials and Processes, second ed.*2007, Berlin.
24. Settefrati, A., et al., *Precipitation sequences in β metastable phase of Ti-5553 alloy during ageing*. Vol. 1. 2011.
25. Bowen, A.W., *Omega phase embrittlement in aged Ti-15%Mo.* Scripta Metallurgica, 1971.
26. Gysler, A., G. Lütjering, and V. Gerold, *Deformation behavior of age-hardened Ti-Mo alloys.* Acta Metallurgica, 1974.
27. Mal'tsev, M.V. and N.V. Petrikova, *Variation in the lattice constant of the beta-phase during isothermal annealing of titanium alloys.* Metal Science and Heat Treatment, 1990.
28. Nag, S., et al., *ω-Assisted nucleation and growth of α precipitates in the Ti–5Al–5Mo–5V–3Cr–0.5Fe β titanium alloy*. Vol. 57. 2009. 2136-2147.
29. Elmer, J.W., et al., *In situ observations of lattice expansion and transformation rates of α and β phases in Ti–6Al–4V.* Materials Science and Engineering: A, 2005.
30. Elmer, J.W., et al., *Low temperature relaxation of residual stress in Ti–6Al–4V.* Scripta Materialia, 2005.
31. Ivasishin, O.M., et al., *Aging response of coarse- and fine-grained β titanium alloys.* Materials Science and Engineering: A, 2005.
32. Mitchell, R., et al., *Characteristics of Electron Beam Welded Ti & Ti Alloys.* Advanced Materials Research, 2011.
33. Carlton, H.D. and J.W. Elmer, *Unpublished results* Lawrence Livermore National Laboratory, 2018.

Table 1. Table reporting on mechanical properties of Ti5553 after different isothermal heat treatments. Only the final heat treatment temperatures are indicated here; all samples experienced a 300°C stress-relief prior to any subsequent treating. N/A indicates the specified quantity could not be defined from the tests performed.

Heat-treatment temperature (°C)	Hardness (HV)	E (GPa)	σ_y (MPa)	σ_u (MPa)	ε to failure (%)
300	291 ± 4	48 ± 1	801 ± 14	824 ± 13	17.2 ± 1.5
400	432 ± 26	66 ± 3	1178 ± N/A	1190 ± 80	1.9 ± 0.1
500	475 ± 20	98 ± 4	N/A	1397 ± 36	1.4 ± 0.1
600	416 ± 16	97 ± 1	1332 ± 32	1371 ± 21	3.5 ± 0.6
700	362 ± 14	92 ± 1	996 ± 17	1088 ± 11	14.2 ± 4.0
800	340 ± 12	78 ± 4	895 ± 39	951 ± 23	15.6 ± 4.5

Table 2. Hydrogen, nitrogen and oxygen were determined by IGF. Aluminum, silicon, vanadium, chromium, iron, molybdenum and titanium were determined by XRF.

Element	Composition
	(Weight %)
Hydrogen (H)	0.0015 ± 0.0002
Nitrogen (N)	0.089 ± 0.001
Oxygen (O)	0.0143 ± 0.0002
Aluminum (Al)	4.8 ± 0.3
Silicon (Si)	0.14 ± 0.03
Vanadium (V)	5.51 ± 0.06
Chromium (Cr)	2.80 ± 0.04
Iron (Fe)	0.34 ± 0.02
Molybdenum (Mo)	5.1 ± 0.3
Titanium (Ti)	Balance; 81.3 ± 0.1

Table 3. Microhardness results of welded Ti5553 showing no change in hardness in the fusion zone or heat affected zone relative to the base metal.

Region of Ti5553 Sample	Hardness Value (Vickers)
AM Base Metal with 300°C stress relief	287± 6.2
Laser Weld Fusion Zone	285 ± 3.9
Laser Weld Heat Affected Zone	281± 3.5

Figures:

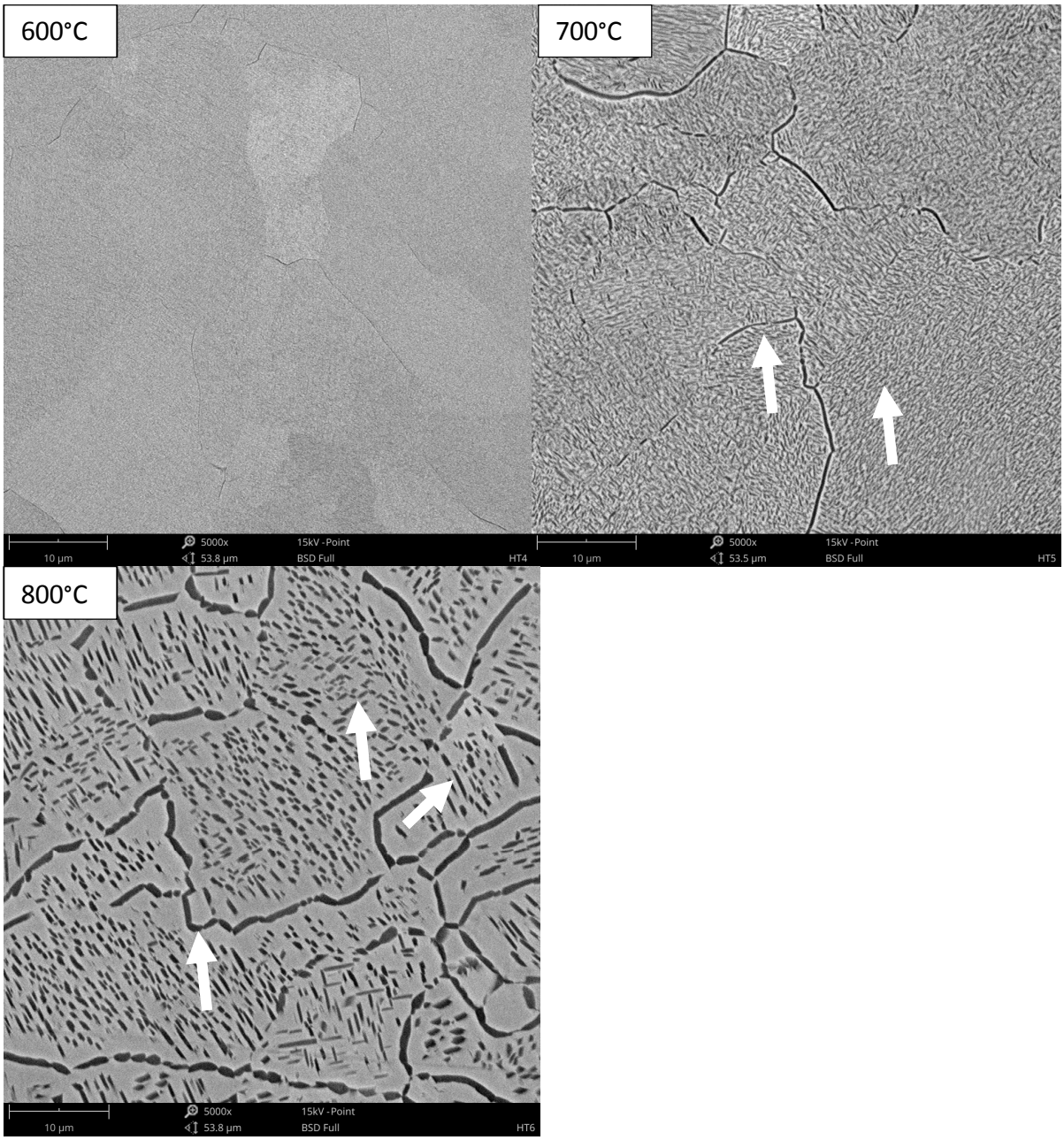

Figure 1. Backscattered electron images showing precipitates of alpha at 600°C with coarsening and morphology changes evident at 700°C and 800°C. The arrows point to alpha phase (dark particles) that are forming on the grain boundaries, and are also dispersed throughout the beta grains.

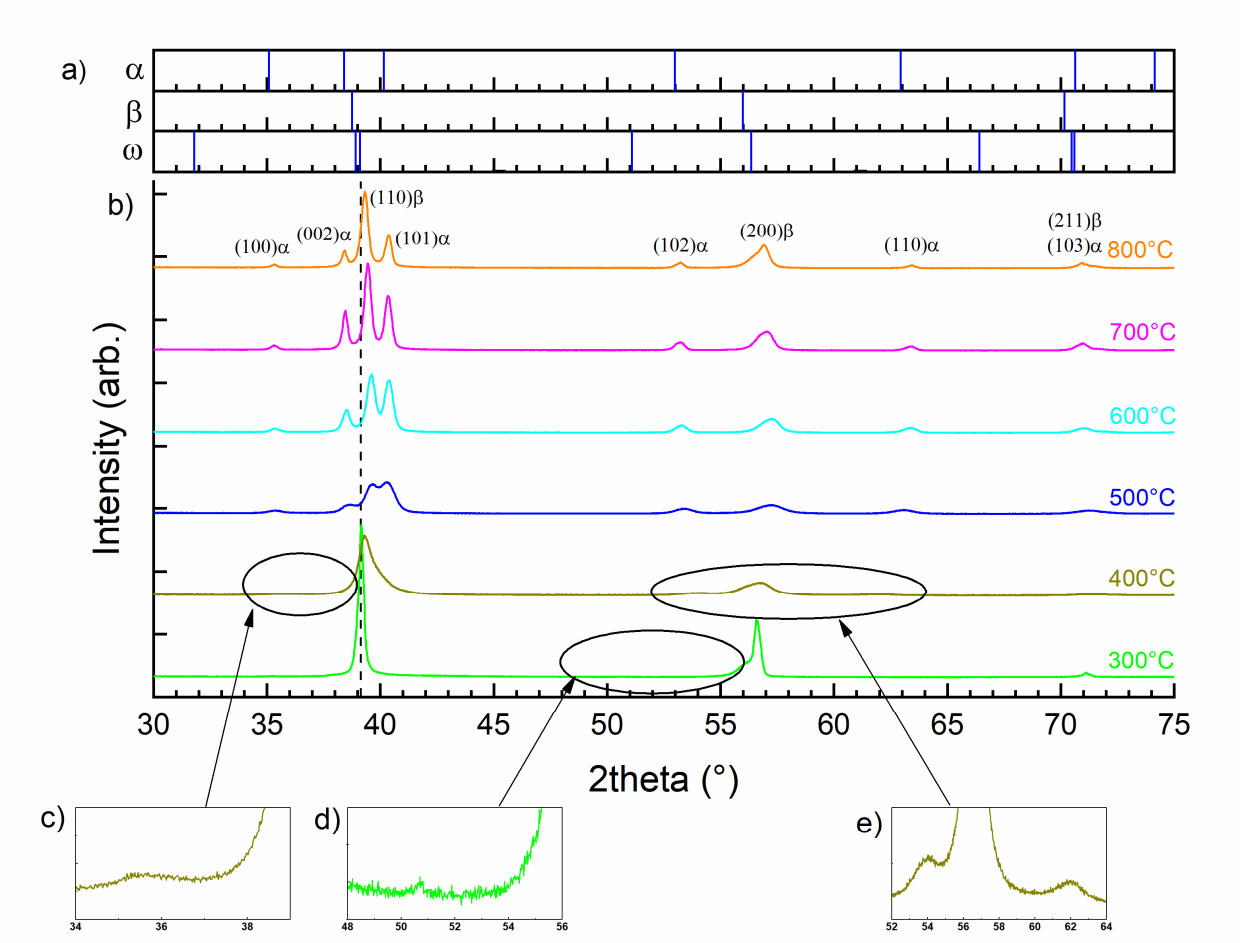

Figure 2. The evolution of the XRD spectrum at different heat treatment temperatures. Locations corresponding to peaks of significant intensity for α (01-089-2762), β (01-089-4913), and ω (04-007-2125) reference PDFs are provided in (a) while the spectra for each heat treatment group are provided in (b). Magnified regions of several angle ranges in the 300°C and 400°C sample spectra are provided in (c)-(e).

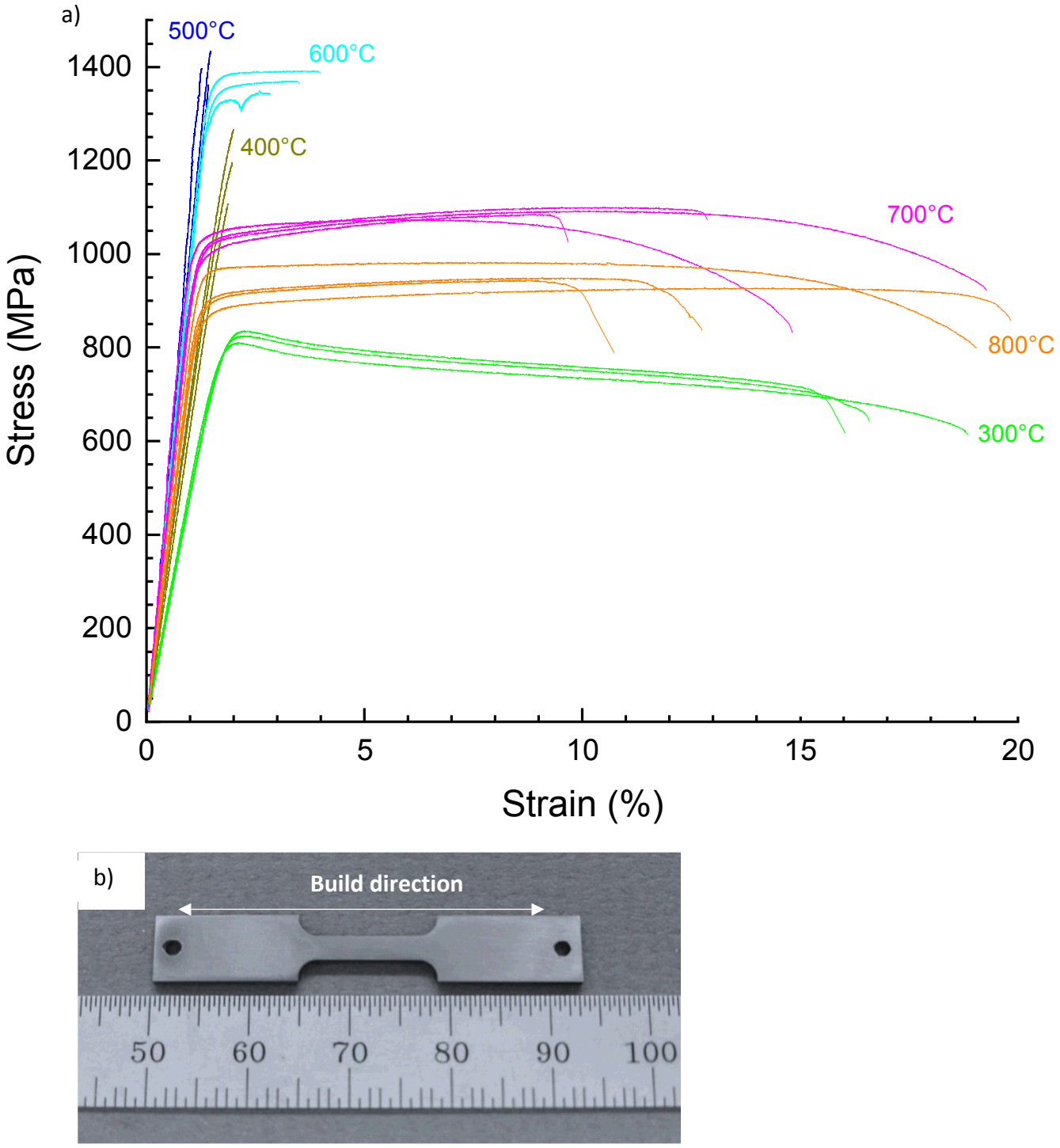

Figure 3. a) Stress vs. strain curves for each of the SLM T5553 different heat treatment sample groups tested tensile specimens. b) Photograph showing a typical tensile specimen and the build direction for the SLM build process (units are in mm).

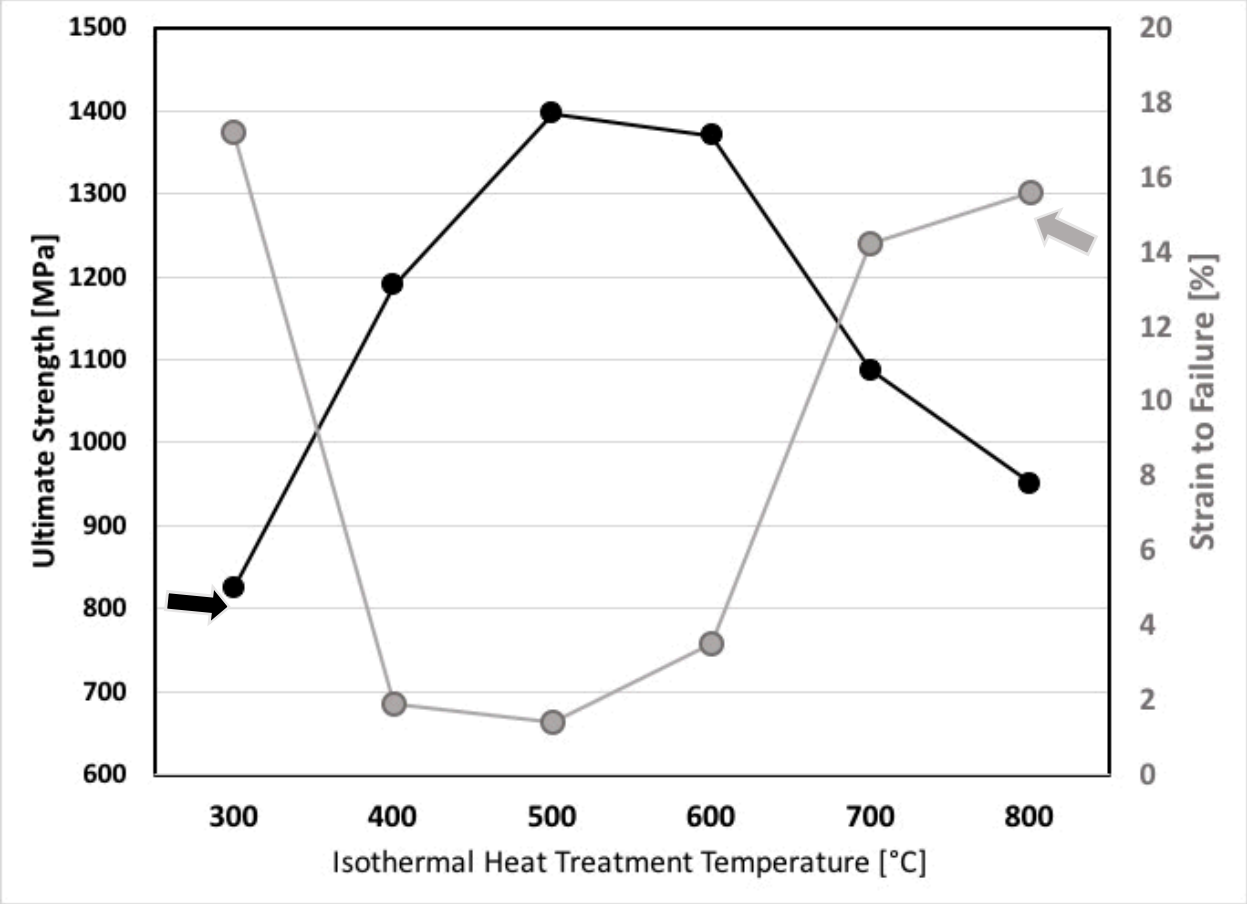

Figure 4. Plot showing the trend of strength and strain to failure as a function of isothermal hold time for the different heat treatments.

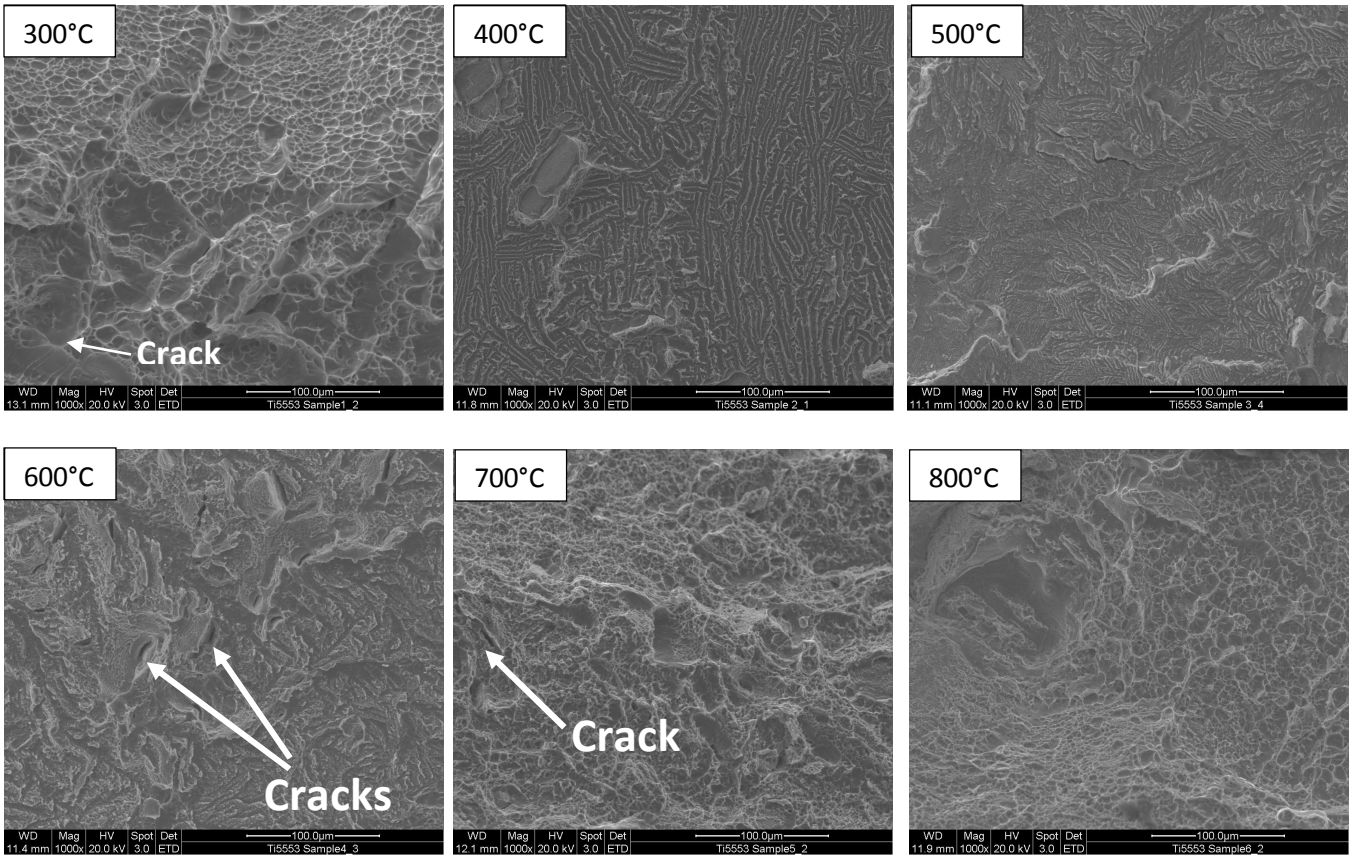

Figure 5. Secondary electron images showing the fractography and changes in failure mode for the different isothermal heat treatments. Significant dimpling indicative of ductile fracture is observed at 300°C and at high temperatures (700°C, 800°C). Ductile dimpling is limited at intermediate temperatures (400-600°C) and a brittle failure mode is evident. Several cracks are also present on the fracture surface which could be initiation sites.

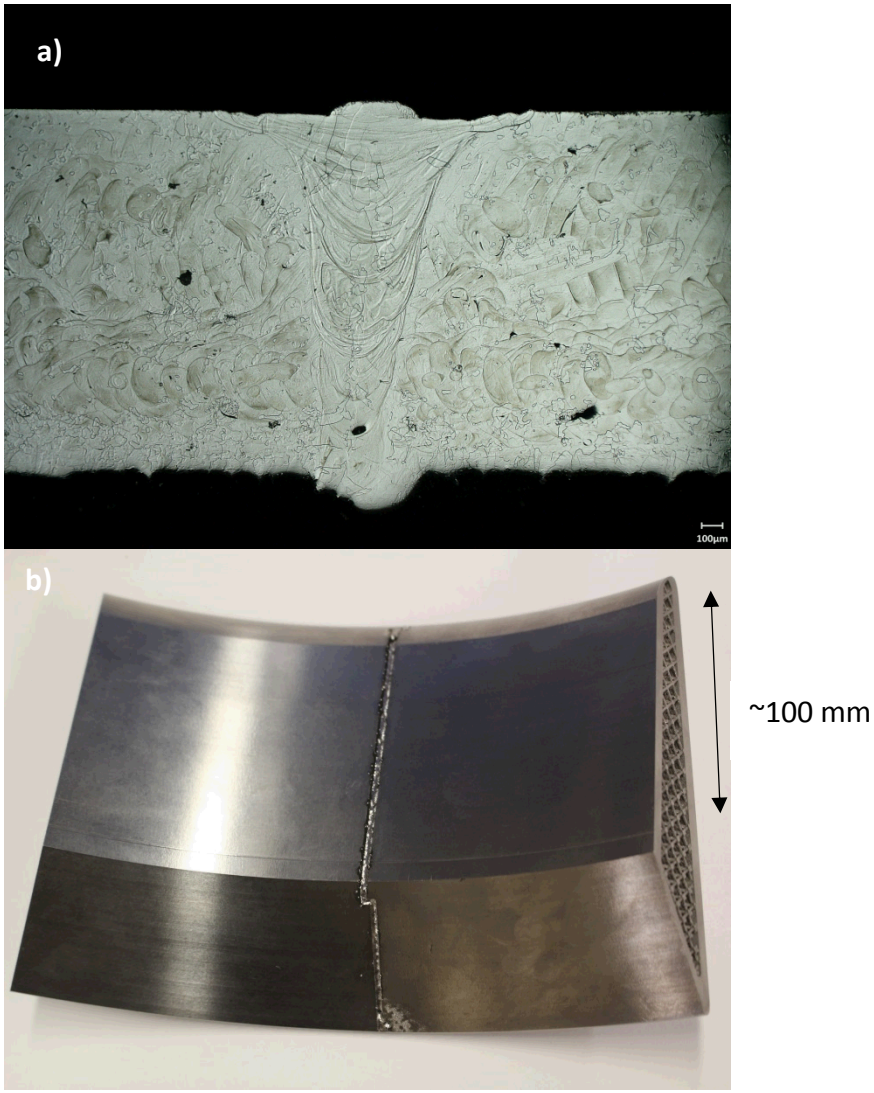

Figure 6. a) Full penetration pulsed laser weld in Ti-5553 AM coupon. Some porosity is present in the AM material that carries into the weld fusion zone. b) Pulsed laser weld joining of two Ti-5553 AM components with an internal lattice structure, prior to final machining of the surface of the part.

ACKNOWLEDGMENTS

The authors would like to thank other LLNL employees who assisted with this work: Stephen Knaus for funding support, John Sengthay, Cheryl Evans, and James Embree for metallographic preparation, Ray Viceral for sample preparation, and Victor Hepa and Dennis Freeman for tensile testing, Ann Mycroft for powder characterization. This work was performed under the auspices of the U.S. Department of Energy by Lawrence Livermore National Laboratory under Contract DE-AC52-07NA27344. This document was prepared as an account of work sponsored by an agency of the United States government. Neither the United States government nor Lawrence Livermore National Security, LLC, nor any of their employees make any warranty, expressed or implied, or assume any legal liability or responsibility for the accuracy, completeness, or usefulness of any information, apparatus, product, or process disclosed, or represent that its use would not infringe privately owned rights. Reference herein to any specific commercial product, process, or service by trade name, trademark, manufacturer, or otherwise does not necessarily constitute or imply its endorsement, recommendation, or favoring by the United States government or Lawrence Livermore National Security, LLC. The views and opinions of authors expressed herein do not necessarily state or reflect those of the United States government or Lawrence Livermore National Security, LLC, and shall not be used for advertising or product endorsement purposes.

Biographical Notes:

Holly D. Carlton, PhD

Holly D. (Barth) Carlton received her PhD in Materials Science and Engineering from the University of California, Berkeley in 2011, after receiving her BS in Engineering Physics and MS in Materials Science and Engineering from the University of California, Berkeley in 2005 and 2008 respectively. She is currently a materials scientist and metallurgist at Lawrence Livermore National Laboratory (LLNL) in the Materials Engineering Division (MED). In 2017, she was awarded the Early Career Recognition Award from LLNL for outstanding research, scientific contribution, and leadership in her field. Her research focuses on investigating the microstructure and mechanical behavior of materials through *in situ* mechanical testing and advanced characterization. One of her recent experiments, where she performed compression tests coupled with synchrotron radiation tomography at Lawrence Berkeley National Laboratory's Advanced Light Source, has been critical in understanding the dominant failure modes in light-weighting structures. Holly was recently the recipient of two prestigious awards from the American Welding Society for advancing knowledge of low alloy steel, stainless steels, and/or surfacing of metals (2015), and for best paper published in the Welding Journal (2016). She has over 20 peer reviewed publications with over 1200 citations and has presented her research at numerous domestic and international conferences.

Kyle Klein

Kyle Klein received his B.S. and M.S. in Materials Science and Engineering from the University of Washington in 2016 and 2017 respectively. He is currently a post-college appointee at Lawrence Livermore National Laboratory (LLNL) in the Materials Engineering Division (MED). Prior to joining the lab, he investigated reaction mechanisms for battery materials during his graduate studies. While at the University of Washington, he also completed a materials engineering internship at PACCAR where he characterized metallic and plastic truck components. His current interests are in metallurgy and the mechanical behavior of materials.

John W. Elmer, ScD, PE, FAWS, FASM, DMTS

John W. Elmer received his ScD in Metallurgical Engineering from the Massachusetts Institute of Technology in 1988, after receiving his BS and MS degrees from the Colorado School of Mines in 1979 and 1981 respectively. He is employed by Lawrence Livermore National Laboratory (LLNL) where he is Distinguished Member of the Technical Staff (DMTS) and leader for the Materials Joining Group of the Materials Engineering Division. Elmer's group is responsible for Materials Joining including laser and electron beam welding, arc welding, vacuum brazing diffusion bonding, soldering and robotic wire arc AM. He has published over 160 technical articles, is a Fellow and Honorary Member of the American Welding Society (AWS), a Fellow of ASM International (ASM), a Senior Member of IEEE, a registered Professional Engineer. Dr. Elmer currently serves on numerous committees for The American Welding Society, ASM International, The Metallurgical Society (TMS), and IEEE. He participates on the editorial review board for The Welding Journal, Metallurgical and Materials Transactions A, and The Science and Technology of Welding and Joining. Dr. Elmer also serves as adjunct professor to the Pennsylvania State University, and visiting scientist at Portland State University.